PERGAMON

International Journal of Solids and Structures 40 (2003) 7155–7179

INTERNATIONAL JOURNAL OF SOLIDS and STRUCTURES

www.elsevier.com/locate/ijsolstr

Debonding of graded coatings under in-plane compression

Tz-Cheng Chiu [a], Fazil Erdogan [b,*]

[a] *SC Packaging Development, Texas Instruments, Inc., 13536 North Central Expressway, MS 940, Dallas, TX 75243, USA*
[b] *Packard Laboratory, Department of Mechanical Engineering and Mechanics, Lehigh University, 19 Memorial Drive West, Bethlehem, PA 18015 3085, USA*

Received 25 September 2002

Abstract

Graded materials are multiphase composites with continuously varying thermophysical properties. The concept provides material scientists and engineers with an important tool to develop new materials tailored for some specific applications. One such application of this new class of materials is as top coats or interfacial regions in thermal barrier systems. A widely observed failure mode in these layered materials is known to be interfacial cracking that leads to spallation. In many cases it is the buckling instability of coating under mechanically or thermally induced compressive stresses that triggers spallation. Under in-plane loading since the linear elastic small deformation theory gives only a trivial solution, in this study the plane strain interface crack problem for a graded coating bonded to a homogeneous substrate is formulated by using a kinematically nonlinear continuum theory. Both the instability and the postbuckling problems are considered. The main objective of the study is the investigation of the influence of material nonhomogeneity, kinematic nonlinearity and plate approximation on the critical instability load and on such fracture mechanics parameters as strain energy release rate, stress intensity factors and crack opening displacements.

Keywords: Fracture mechanics; Graded materials; Thermal barrier coatings; Buckling instability; Spallation

1. Introduction

A common failure mode in thermal barrier and a variety of other coatings is known to be interface cracking that leads to spallation. Depending on the relative values of thermal expansion coefficients of the coating and the substrate and the nature of the mechanical loading applied to the system, the in-plane stresses in the coating may be tensile or compressive, invariably cyclic. In the case of tensile stresses the fracture mechanism is rather straightforward: initiation of microcracks on the coating surface, subcritical growth of a dominant crack through the coating, and formation and growth of a T-shaped crack along the coating-substrate interface. On the other hand, particularly in the case of ceramic coatings, the spallation fracture appears to be due to in-plane cyclic compression (Evans and Hutchinson, 1984). The process starts by the formation and coalescence of microcracks at or near the interface asperities under cyclic loading

* Corresponding author. Tel.: +1-610-758-4100; fax: +1-610-758-6224.
E-mail address: fe00@lehigh.edu (F. Erdogan).

0020-7683/$ - see front matter © 2003 Elsevier Ltd. All rights reserved.
doi:10.1016/S0020-7683(03)00360-3

(Evans et al., 1997; Nusier and Newaz, 1998; Evans et al., 1983). Thus, as a consequence of a fully formed interface crack or a highly weakened interface the coating buckles or blisters under a peak compressive load (e.g., Chai et al., 1983; Bottega and Maewal, 1983; Peck and Springer, 1991; Hutchinson and Suo, 1992; Garg, 1988). In the past the studies dealing with the postbuckling analysis of coatings and thin films as well as with the determination of buckling instability load were carried out by using an appropriate plate theory and certain assumptions regarding the boundary conditions. A number of studies have also been carried out on buckling instability for embedded cracks within the context of two dimensional continuum (Keer et al., 1982; Wang et al., 1991; Wang and Takao, 1995; Madenci and Westmann, 1991). Because of the nonlinear nature of the problem finite element methods have also been used rather extensively in investigating the general problem of buckling and delamination growth in coating/substrate systems (e.g., Nilsson and Giannakopoulos, 1990; Nilsson et al., 1993; Whitcomb, 1989).

In the process of interface crack growth leading to spallation fracture, at first the crack is driven subcritically in a co-planar fashion. Then, upon reaching the critical condition at the crack tip a mixed-mode fracture occurs, exposing the interface to an undesirable thermal or chemical environment. In most studies on the subject the objective, therefore, has been the evaluation of the crack driving force for a given interface crack and a thermomechanical loading system. For in-plane compression since the infinitesimal theory of elasticity would give only a trivial solution (that is, no crack opening) the problem must be treated by using a kinematically nonlinear theory (Chiu, 2000). In previous studies involving buckling instability and postbuckling analysis the underlying mechanics problems have been solved by using the von Karman plate theory and by assuming that the layered medium is piecewise homogeneous (e.g., Hutchinson and Suo, 1992). This so-called buckle-driven delamination has also been considered by Bao and Cai (1997) for a graded coating bonded to a semi-infinite homogeneous substrate and containing a crack parallel to the interface. The related postbuckling problem for the plate with graded properties was solved by using the technique described by Hutchinson and Suo (1992). [1] Coatings designed to protect the substrate against severe thermal and chemical environments are invariably ceramics. In such applications ceramics, however, seem to have certain undesirable properties, namely brittleness, poor bonding strength and high residual and thermal stresses. They are, therefore, highly susceptible to cracking and spallation. An alternative concept that may be used to overcome some of these shortcomings of the homogeneous ceramic coatings appears to be the through-thickness grading of the thermophysical properties of coatings (Miyamoto et al., 1999). Graded materials, also known as *functionally graded materials* (FGMs), are generally two phase composites with continuously varying volume fractions or compositions. Used as coatings and interfacial zones they tend to reduce stresses resulting from the material property mismatch, increase the bonding strength, improve the surface properties and provide protection against adverse thermal and chemical environments. Thus the concept provides the material scientists and engineers with an important tool to design new materials for some specific applications. For a comprehensive review of the design, processing and applications of graded materials and for extensive references (see Yamanouchi et al., 1990; Holt et al., 1993; Ilschner and Cherradi, 1995; Shiota and Miyamoto, 1997; Kaysser, 1999; Trumble et al., 2001).

Aside from some useful physical properties mentioned above, the graded materials have also certain analytical advantages, that is, by eliminating material property discontinuities some well known mathematical anomalies associated with the bonded dissimilar materials are also eliminated. These are the complex singularities for the interface cracks, nonsquare-root singularities for cracks terminating at the interfaces and weak power singularities at the points of intersection of free surfaces and interfaces. Thus, in studying the fracture mechanics of graded materials by using, for example, a standard finite element procedure, the calculation of the strain energy release rate and the stress intensity factors becomes quite straightforward.

[1] At the request of the reviewer and for completeness the technique is also briefly outlined in an Appendix A to this article.

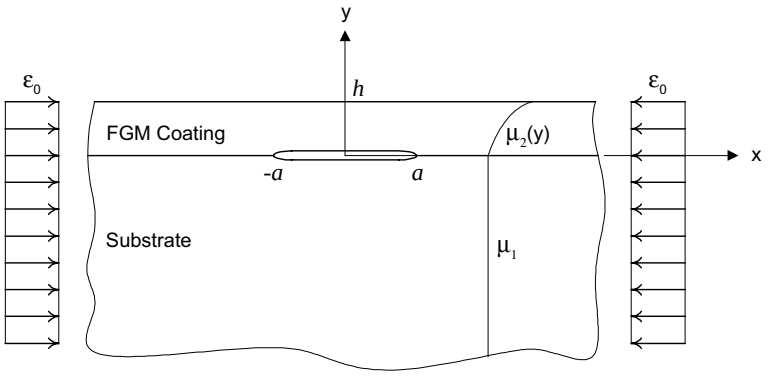

Fig. 1. Graded coating bonded to a homogeneous substrate with an interface crack subjected to uniform compressive strain.

Despite the fact that the concept of material property grading is relatively new, [2] it has a wide range of potentially very useful and technologically very important applications. Following are some of these applications the feasibility of which has been demonstrated: high temperature resistant coatings; coatings on load transfer components (e.g., gears, bearings and other contacting elements); impact-resistant surface layers; interfacial zones with high bonding strength; thermoelectric cells with improved thermal efficiency; and graded index optical glass and polymer fibers for high speed data transmission (mostly in local area networks).

2. Description of the problem

In actual applications such as gas turbines, combustion chambers and high speed civil transport, the thermal barrier system consists of a ceramic top coat (the primary heat shield), a very thin layer of thermally grown oxide which developes during operation and a bond coat deposited over the substrate to prevent oxygen diffusion. Also the debonded region is most likely circular or elliptic. In this study we consider a somewhat idealized version of the problem which is shown in Fig. 1. It is assumed that the dimensions of the substrate are very large in comparison with the coating thickness h and the length $2a$ of the interface crack. Thus, the plane strain problem under consideration consists of a graded coating bonded to a homogeneous, isotropic semi-infinite substrate. The composite medium is subjected to remote in-plane (fixed-grip) compression

$$\epsilon_{1xx}(\mp\infty, y) = -\epsilon_0, \quad -\infty < y < 0, \qquad \epsilon_{2xx}(\mp\infty, y) = -\epsilon_0, \quad 0 < y < h, \tag{1}$$

where the subscripts 1 and 2 refer to materials 1 (substrate) and 2 (coating), respectively. In previous studies it was shown that the influence of the variation in Poisson's ratio ν for crack problems in graded materials is rather insignificant (Delale and Erdogan, 1988; Chen and Erdogan, 1996) and ν may be assumed to be constant throughout the medium. It is further assumed that the material nonhomogeneity in the coating may be expressed by

$$\mu_2(y) = \mu_1 e^{\gamma y}, \quad 0 < y < h, \tag{2}$$

where μ_1 is the shear modulus of the substrate which is constant and the dimensionless parameter γh is the measure of material nonhomogeneity.

[2] The phrase functionally graded material (FGM) and the underlying concept were first proposed by M. Niino and the first successful manufacture of a graded material (superalloy/ceramic for high temperature resistance) was described by Niino et al. (1987).

Again from Fig. 1 observing that the solution given by the linear continuum modeling of the medium is of no physical consequence, in this study the problems of buckling instability and postbuckling analysis need to be treated by using a kinematically nonlinear continuum model. The main objectives of this study are, then, (i) to examine the limitations of the plate approximation by comparing the results obtained from the von Karman plate theory and the nonlinear elasticity, (ii) to investigate the influence of the material property grading in the coating on the stress intensity factors, the strain energy release rate, the crack opening displacement and the buckling instability load, and (iii) to carry out the necessary postbuckling analysis.

3. The buckling instability problem for graded coatings

3.1. The formulation

In the absence of body forces the equations of finite deformation theory of elasticity may be expressed as (e.g., Malvern, 1969)

$$\sigma_{ij,j} + (\sigma_{jk}u_{i,k})_{,j} = 0, \tag{3}$$

$$(\sigma_{ij} + \sigma_{jk}u_{i,k})n_j = T_i, \tag{4}$$

where u_i, σ_{ij}, T_i, and n_i, $(i,j) = (1,2,3)$, are, respectively, the components of the displacement, second Piola–Kirchhoff stress, surface traction and unit normal vector. Note that (3) and (4) are referenced to a fixed Cartesian coordinate system under the Lagrangian description of deformations. The Green–Lagrange strains are then given by

$$\epsilon_{ij} = \tfrac{1}{2}(u_{i,j} + u_{j,i} + u_{k,i}u_{k,j}). \tag{5}$$

For the stability analysis (3)–(5) may be reduced to a linearized set of equations by using a standard perturbation technique (or the adjacent equilibrium concept). It is assumed that at bifurcation a critical equilibrium configuration exists which in the sequel is denoted by the superscript (0). The displacements, stresses, tractions and strains for an adjacent or buckled configuration may then be expressed as follows:

$$u_i = u_i^{(0)} + u_i^*, \quad \sigma_{ij} = \sigma_{ij}^{(0)} + \sigma_{ij}^*, \quad T_i = T_i^{(0)} + T_i^*, \quad \epsilon_{ij} = \epsilon_{ij}^{(0)} + \epsilon_{ij}^*, \tag{6a–d}$$

where the asterisk denotes the perturbation or a small deviation from the critical equilibrium configuration. Thus, by substituting from (6) into (3)–(5) and neglecting the higher order terms we obtain the following system of linear equations

$$\sigma_{ij,j}^* + (\sigma_{jk}^{(0)}u_{i,k}^*)_{,j} = 0, \tag{7}$$

$$(\sigma_{ij}^* + \sigma_{jk}^{(0)}u_{i,k}^*)n_j = T_i^*, \tag{8}$$

$$\epsilon_{ij}^* = \tfrac{1}{2}(u_{i,j}^* + u_{j,i}^*). \tag{9}$$

For the plane strain problem described by Fig. 1, the in-plane strain ϵ_0 is the only applied load in terms of which the initial equilibrium state at bifurcation is found to be

$$\epsilon_{ixx}^{(0)} = -\epsilon_0, \quad \sigma_{iyy}^{(0)} = 0, \quad \sigma_{ixy}^{(0)} = 0, \quad \epsilon_{ixy}^{(0)} = 0, \quad \epsilon_{iyy}^{(0)} = \left(\frac{3-\kappa_i}{\kappa_i+1}\right)\epsilon_0, \quad \sigma_{ixx}^{(0)} = -\frac{8\mu_i\epsilon_0}{\kappa_i+1} \qquad (i=1,2), \tag{10a–f}$$

where $i = 1,2$ refer to materials 1 (the substrate) and 2 (the coating), respectively, and $\kappa = 3–4\nu$. By using the kinematic relations (9), the Hooke's law

$$\sigma^*_{xx} = \left(\frac{\kappa+1}{\kappa-1}\right)\mu\epsilon^*_{xx} + \left(\frac{3-\kappa}{\kappa-1}\right)\mu\epsilon^*_{yy},$$
$$\sigma^*_{yy} = \left(\frac{3-\kappa}{\kappa-1}\right)\mu\epsilon^*_{xx} + \left(\frac{\kappa+1}{\kappa-1}\right)\mu\epsilon^*_{yy}, \tag{11a–c}$$
$$\sigma^*_{xy} = 2\mu\epsilon^*_{xy},$$

and the relations expressing the material nonhomogeneity

$$\mu_i(y) = \mu_{i0}e^{\gamma_i y}, \quad i = 1, 2, \tag{12}$$

from (7) it may be shown that

$$(\kappa+1)\frac{\partial^2 u^*_i}{\partial x^2} + (\kappa-1)\frac{\partial^2 u^*_i}{\partial y^2} + 2\frac{\partial^2 v^*_i}{\partial x\partial y} + \gamma_i(\kappa-1)\left(\frac{\partial u^*_i}{\partial y} + \frac{\partial v^*_i}{\partial x}\right) - 8\left(\frac{\kappa-1}{\kappa+1}\right)\epsilon_0\frac{\partial^2 u^*_i}{\partial x^2} = 0, \quad i = 1, 2,$$

$$(\kappa-1)\frac{\partial^2 v^*_i}{\partial x^2} + (\kappa+1)\frac{\partial^2 v^*_i}{\partial y^2} + 2\frac{\partial^2 u^*_i}{\partial x\partial y} + \gamma_i(3-\kappa)\frac{\partial u^*_i}{\partial x} + \gamma_i(\kappa+1)\frac{\partial v^*_i}{\partial y} - 8\left(\frac{\kappa-1}{\kappa+1}\right)\epsilon_0\frac{\partial^2 v^*_i}{\partial x^2} = 0, \quad i = 1, 2, \tag{13a,b}$$

where $\mu_{10} = \mu_{20} = \mu_1$, $\gamma_1 = 0$, $\gamma_2 = \gamma$, and u_i and v_i are the x and y components of the displacement, the subscript $i = 1, 2$ representing the materials 1 and 2. The equilibrium equations (13) must be solved under the following boundary and continuity conditions:

$$\sigma^*_{2yy}(x, h) = 0, \quad \sigma^*_{2xy}(x, h) = 0, \qquad -\infty < x < \infty, \tag{14a,b}$$

$$\sigma^*_{2yy}(x, +0) = \sigma^*_{1yy}(x, -0), \quad \sigma^*_{2xy}(x, +0) = \sigma^*_{1xy}(x, -0), \qquad -\infty < x < \infty, \tag{15a,b}$$

$$\sigma^*_{1yy}(x, -0) = 0, \quad \sigma^*_{1xy}(x, -0) = 0, \qquad -a < x < a, \tag{16a,b}$$

$$u^*_1(x, -0) = u^*_2(x, +0), \quad v^*_1(x, -0) = v^*_2(x, +0), \qquad |x| > a. \tag{17a,b}$$

From (13) it may be seen that for $\gamma = 0$ the problem reduces to a stability problem for a homogeneous half plane with a crack parallel to its boundary. Similarly, for $\epsilon_0 = 0$ we obtain the standard equations elastostatics for a nonhomogeneous medium. It should be emphasized that in the problem under consideration both the differential equation (13) and the boundary conditions (14)–(17) are homogeneous. Thus, the system constitutes a typical eigenvalue problem of the form

$$L(\underset{\sim}{u}) = \lambda N(\underset{\sim}{u}) \tag{18}$$

subject to appropriate homogeneous boundary conditions where u and λ represent the displacements and the applied load ϵ_0, respectively. Thus, aside from a null solution Eqs. (13)–(17) would admit a nonzero solution only for a discrete set of eigenvalues ϵ_{0i}, $i = 1, 2, \ldots$, the lowest nonzero eigenvalue being the critical load $(\epsilon_0)_{cr}$.

To determine $(\epsilon_0)_{cr}$ and the fracture mechanics parameters we simply proceed with the solution of the mixed boundary value problem formulated by (13)–(17). By using the standard Fourier transforms, for the substrate $(i = 1)$ from (13) we obtain

$$u_1^*(x,y)=\frac{1}{2\pi}\int_{-\infty}^{\infty}(A_1e^{\lambda_1 y}+A_2e^{\lambda_2 y})e^{i\alpha x}\,d\alpha,$$
$$v_1^*(x,y)=\frac{1}{2\pi}\int_{-\infty}^{\infty}\left(\frac{\alpha}{i\lambda_1}A_1e^{\lambda_1 y}+\frac{\lambda_2}{i\alpha}A_2e^{\lambda_2 y}\right)e^{i\alpha x}\,d\alpha, \tag{19a,b}$$

$$\lambda_1=\left(1-\frac{8\epsilon_0}{\kappa+1}\right)^{1/2}|\alpha|,\quad \lambda_2=\left[1-\frac{8(\kappa-1)\epsilon_0}{(\kappa+1)^2}\right]^{1/2}|\alpha|, \tag{20a,b}$$

where A_1 and A_2 are unknown functions of α. Similarly, for the graded coating (Eq. (13), $i=2$) we find

$$u_2^*(x,y)=\frac{1}{2\pi}\int_{-\infty}^{\infty}\sum_{k=1}^{4}C_k(\alpha)e^{n_k y}e^{i\alpha x}\,d\alpha,$$
$$v_2^*(x,y)=\frac{1}{2\pi}\int_{-\infty}^{\infty}\sum_{k=1}^{4}m_k(\alpha)C_k(\alpha)e^{n_k y}e^{i\alpha x}\,d\alpha, \tag{21a,b}$$

where $C_1,\ldots,C_4$ are unknown, $n_1,\ldots,n_4$ are the roots of the characteristic equation resulting from (13) and are found to be

$$n_1=-\frac{\gamma}{2}-\sqrt{\frac{\gamma^2}{4}+\alpha^2\left[1-\frac{8\kappa\epsilon_0}{(\kappa+1)^2}\right]+\alpha\sqrt{\alpha^2\frac{(8\epsilon_0)^2}{(\kappa+1)^4}-\gamma^2\left(\frac{3-\kappa}{\kappa+1}\right)}},$$
$$n_2=-\frac{\gamma}{2}-\sqrt{\frac{\gamma^2}{4}+\alpha^2\left[1-\frac{8\kappa\epsilon_0}{(\kappa+1)^2}\right]-\alpha\sqrt{\alpha^2\frac{(8\epsilon_0)^2}{(\kappa+1)^4}-\gamma^2\left(\frac{3-\kappa}{\kappa+1}\right)}},$$
$$n_3=-\frac{\gamma}{2}+\sqrt{\frac{\gamma^2}{4}+\alpha^2\left[1-\frac{8\kappa\epsilon_0}{(\kappa+1)^2}\right]+\alpha\sqrt{\alpha^2\frac{(8\epsilon_0)^2}{(\kappa+1)^4}-\gamma^2\left(\frac{3-\kappa}{\kappa+1}\right)}}, \tag{22a–d}$$
$$n_4=-\frac{\gamma}{2}+\sqrt{\frac{\gamma^2}{4}+\alpha^2\left[1-\frac{8\kappa\epsilon_0}{(\kappa+1)^2}\right]-\alpha\sqrt{\alpha^2\frac{(8\epsilon_0)^2}{(\kappa+1)^4}-\gamma^2\left(\frac{3-\kappa}{\kappa+1}\right)}}$$

and the coefficients $m_1,\ldots,m_4$ are given by

$$m_k(\alpha)=\frac{-i\alpha[2n_k+\gamma(3-\kappa)]}{(\kappa+1)n_k^2+\gamma(\kappa+1)n_k-\left[(\kappa-1)-8\left(\frac{\kappa-1}{\kappa+1}\right)\epsilon_0\right]\alpha^2},\quad k=1,\ldots,4. \tag{23}$$

Four of the six unknowns A_j, $(j=1,2)$ and C_k, $(k=1,\ldots,4)$ may be eliminated by substituting from (9), (11), (19) and (21) into the homogeneous conditions (14) and (15). The remaining two unknowns may then be determined from the mixed boundary conditions (16) and (17).

3.2. The integral equations

By defining the following unknown functions

$$f_1(x)=\frac{\partial}{\partial x}[v_2^*(x,+0)-v_1^*(x,-0)],$$
$$f_2(x)=\frac{\partial}{\partial x}[u_2^*(x,+0)-u_1^*(x,-0)],\qquad -\infty<x<\infty \tag{24a,b}$$

and from (17) observing that

$$f_1(x) = 0, \quad f_2(x) = 0, \qquad |x| > a, \tag{25a,b}$$

after somewhat lengthy but straightforward manipulations and after performing the necessary asymptotic analysis, the mixed boundary conditions (16) and (17) may be reduced to

$$\frac{\mu_1}{\pi}\int_{-a}^{a}\sum_{j=1}^{2}\left[\frac{D_i\delta_{ij}}{t-x}+k_{ij}(x,t)\right]f_j(t)\,\mathrm{d}t = 0, \quad i = 1,2, \ \ |x| < a, \tag{26}$$

where $k_{ij}(x,t)$, $(i,j=1,2)$ are known functions (see Chiu (2000) for complete details and extensive results) and the constants D_1 and D_2 are given by

$$D_1 = \frac{\left(1-\frac{8\epsilon_0}{\kappa+1}\right)^{1/2}\left[1-\frac{8(\kappa-1)\epsilon_0}{(\kappa+1)^2}\right]^{1/2}-\left(1-\frac{4\epsilon_0}{\kappa+1}\right)^2}{\frac{4\epsilon_0}{\kappa+1}\left[1-\frac{8(\kappa-1)\epsilon_0}{(\kappa+1)^2}\right]^{1/2}},$$
$$D_2 = \frac{\left(1-\frac{8\epsilon_0}{\kappa+1}\right)^{1/2}\left[1-\frac{8(\kappa-1)\epsilon_0}{(\kappa+1)^2}\right]^{1/2}-\left(1-\frac{4\epsilon_0}{\kappa+1}\right)^2}{\frac{4\epsilon_0}{\kappa+1}\left(1-\frac{8\epsilon_0}{\kappa+1}\right)^{1/2}}. \tag{27a,b}$$

From the definition (24) and conditions (17) it follows that the integral equations (26) must be solved under the following single-valuedness conditions

$$\int_{-a}^{a} f_i(t)\,\mathrm{d}t = 0, \quad i = 1,2. \tag{28}$$

It should again be observed that in the instability problem under consideration the integral equations (26) as well as the auxiliary conditions (28) are homogeneous and normally $f_1 = 0$ and $f_2 = 0$ would be the only solution. However, the kernels in (26) are very complicated functions of the variable loading parameter ϵ_0. The problem is, therefore, an eigenvalue problem and for certain discrete set of positive values of ϵ_0 it may admit nonzero solutions.

3.3. The problem of highly damaged interface

The forgoing analysis is based on the assumption that a through crack exists along the x axis ($-a < x < a$, $y = 0$, Fig. 1). In some cases, however, one may have only a highly weakened interfacial region rather than complete rupture. The damaged region may be modeled as a series of small interface cracks separated by weak unbroken ligaments shown in Fig. 2. In the model adopted in this study it is assumed that the ligaments may be represented by a pair of tension and shear springs. Thus, the problem of a series of small collinear cracks may be replaced by that of a macroscopic crack ($-a < x < a$, $y = 0$) the surfaces of which are connected by springs with continuously distributed coefficients s_1 and s_2 (Fig. 2). From Figs. 1 and 2 it may be seen that in the highly damaged interface problem the Eqs. (13), (14), (15) and (17) are still valid, but (16) must be replaced by a pair of conditions that account for the crack surface bridging effect. For simplicity here it will be assumed that the bridging stresses are proportional to the relative crack openings, that is the springs are assumed to be linear. Thus, the conditions that replace (16) become

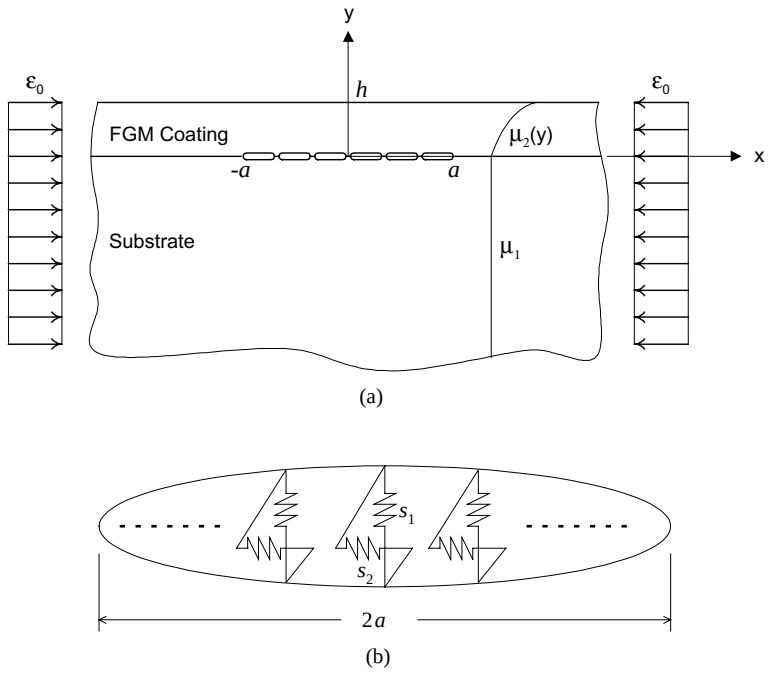

Fig. 2. (a) Graded coating bonded to a homogeneous substrate with a weakened interfacial region subjected to uniform compressive strain. (b) Tension and shear springs modeling crack surface ligaments.

$$\sigma^*_{1yy}(x,-0) = s_1[v_2(x,+0) - v_1(x,-0)], \quad \sigma^*_{1xy}(x,-0) = s_2[u_2(x,+0) - u_1(x,-0)], \quad |x| < a, \tag{29a,b}$$

where s_1 and s_2 are known constants. From (17) and (24) the crack opening displacements may be expressed as

$$v_2(x,+0) - v_1(x,-0) = \int_{-a}^{x} f_1(t)\,\mathrm{d}t, \quad |x| < a,$$
$$u_2(x,+0) - u_1(x,-0) = \int_{-a}^{x} f_2(t)\,\mathrm{d}t, \quad |x| < a. \tag{30a,b}$$

Noting that in the problem (29a) and (29b) are the crack surface tractions, taking into account (29) and (30), the integral equations (26) will have to be modified as

$$\frac{\mu_1}{\pi}\int_{-a}^{a}\sum_{j=1}^{2}\left[\frac{D_i\delta_{ij}}{t-x} + k_{ij}(x,t)\right]f_j(t)\,\mathrm{d}t - s_i\int_{-a}^{x} f_i(t)\,\mathrm{d}t = 0, \quad i = 1,2, \ \ |x| < a. \tag{31}$$

Eqs. (31), too, must be solved under the single-valuedness conditions (28). We again observe that both (31) and (28) are homogeneous and consequently the system constitutes an eigenvalue problem.

It should be noted that as long as the "applied load" ϵ_0 is less than a critical value $(\epsilon_0)_{\mathrm{cr}}$ the crack surfaces remain closed. The springs s_1 and s_2 that provide the crack surface bridging are assumed to be linear. Consequently the eigenvalue problem formulated by (31) and (28) remains to be also linear. The problem becomes nonlinear during the postbuckling phase of the loading $\epsilon_0 > (\epsilon_0)_{\mathrm{cr}}$. The eigenvalue

problem becomes also nonlinear if the bridging forces applied by the ligaments are modeled in a physically more realistic manner (see, for example, Erdogan and Joseph (1989)).

3.4. On the solution of integral equations

To solve the integral equations (26) and (31), first the following normalized quantities are defined

$$s = t/a, \quad r = x/a, \qquad -1 < (s,r) < 1, \tag{32}$$

$$F_i(s) = f_i(t), \quad K_{ij}(r,s) = ak_{ij}(x,t), \qquad i,j = 1,2. \tag{33}$$

Eqs. (26), (31) and (28) then become

$$\frac{\mu_1}{\pi}\int_{-1}^{1}\sum_{j=1}^{2}\left[\frac{D_i\delta_{ij}}{s-r}+K_{ij}(r,s)\right]F_j(s)\,\mathrm{d}s = 0, \quad i = 1,2, \ -1 < r < 1, \tag{34}$$

$$\frac{\mu_1}{\pi}\int_{-1}^{1}\sum_{j=1}^{2}\left[\frac{D_i\delta_{ij}}{s-r}+K_{ij}(r,s)\right]F_j(s)\,\mathrm{d}s - as_i\int_{-1}^{r}F_i(s)\,\mathrm{d}s = 0, \quad i = 1,2, \ -1 < r < 1, \tag{35}$$

$$\int_{-1}^{1}F_i(s)\,\mathrm{d}s = 0, \quad i = 1,2. \tag{36}$$

It may easily be shown that the index of (34) and (35) is +1 and their solutions are of the form

$$F_i(s) = \frac{g_i(s)}{\sqrt{1-s^2}}, \quad -1 < s < 1, \ i = 1,2. \tag{37}$$

The bounded unknown functions $g_1(s)$ and $g_2(s)$ are Hölder-continuous and $g_i(-1) \neq 0$, $g_i(+1) \neq 0$, $i = 1, 2$. These functions can be expressed in terms of infinite series of orthogonal polynomials associated with the weight function $(1-s^2)^{-1/2}$ (in this case the Chebyshev polynomials of the first kind $T_n(s)$, $n = 0, 1, \ldots$). Truncating the series and considering the following symmetry properties of T_n, v_i and u_i

$$F_1(s) = -F_1(-s), \quad F_2(s) = F_2(-s), \tag{38}$$

$$T_{2n-1}(s) = -T_{2n-1}(-s), \quad T_{2n}(s) = T_{2n}(-s), \qquad n = 0,1,\ldots \tag{39}$$

the unknown functions F_1 and F_2 may be approximated as follows:

$$F_1(s) \cong \frac{1}{\sqrt{1-s^2}}\sum_{n=1}^{N}B_nT_{2n-1}(s), \tag{40}$$

$$F_2(s) \cong \frac{1}{\sqrt{1-s^2}}\sum_{n=1}^{N}B_{N+n}T_{2n}(s). \tag{41}$$

From the orthogonality conditions of $\mathrm{T}_n(s)$ it follows that (40) and (41) satisfy the single-valuedness conditions (36) identically. The unknown coefficients B_n, $n = 1, \ldots, 2N$, may then be determined by substituting from (40) and (41) into the integral equations (34) or (35). Thus, by using the relations

$$\frac{1}{\pi}\int_{-1}^{1}\frac{\mathrm{T}_k(s)\,\mathrm{d}s}{(s-r)\sqrt{1-s^2}}=\begin{cases}0, & k=0,\ |r|<1,\\ U_{k-1}(r), & k>0,\ |r|<1,\\ -\dfrac{\left(r-\frac{|r|}{r}\sqrt{r^2-1}\right)^k}{\left(\frac{|r|}{r}\sqrt{r^2-1}\right)}, & k\geqslant 0,\ |r|>1,\end{cases} \tag{42}$$

$$\int_{-1}^{1}\frac{T_k(s)}{\sqrt{1-s^2}}\log|s-r|\,\mathrm{d}s=-\frac{\pi}{k}T_k(r),\quad k\geqslant 1, \tag{43}$$

$$\int_{-1}^{1}\frac{T_k(s)}{\sqrt{1-s^2}}\frac{|s-r|}{s-r}\,\mathrm{d}s=\frac{2}{k}U_{k-1}(r)\sqrt{1-r^2},\quad k\geqslant 1 \tag{44}$$

to regularize the integrals involving Cauchy and logarithmic singularities and the discontinuous behavior in the kernels and by performing the remaining integrals, the singular integral equations (34) and (35) may be reduced to a functional equation of the form

$$\sum_{j=1}^{2N}G_j(r,\epsilon_0)B_j=0. \tag{45}$$

In (42) and (44) $U_k(r)$ is the Chebyshev polynomial of the second kind. We again note that in (34) and (35) D_i and K_{ij} are functions of the variable load parameter ϵ_0. Consequently the coefficients G_j and through which B_j and the original unknown functions f_1 and f_2 are also functions of ϵ_0. Eq. (45) may be solved for B_j by using a standard weighted residual technique. For example, using a collocation technique, (45) may be reduced to

$$\sum_{j=1}^{2N}c_{ij}(\epsilon_0)B_j=0,\quad c_{ij}(\epsilon_0)=G_j(r_i,\epsilon_0),\qquad i=1,\ldots,2N. \tag{46}$$

Aside from the trivial solution $B_j=0$, $j=1,\ldots,2N$, a nonzero solution of (46) exists for values of ϵ_0 satisfying

$$|c_{ij}(\epsilon_0)|=0\quad(i,j=1,\ldots,2N). \tag{47}$$

The smallest positive root of (47) ϵ_{01} is the critical instability load $(\epsilon_0)_{\mathrm{cr}}$ and the corresponding eigenvector B_{1j} would give the fundamental buckling mode.

3.5. Crack opening displacements and stress intensity factors

After determining B_j from (30a), (30b), (40) and (41) the crack opening displacements may be evaluated as follows:

$$\begin{aligned}v_2(x,+0)-v_1(x,-0)&=-\sum_{k=1}^{N}B_{1k}\frac{U_{2k-2}(x/a)}{2k-1}\sqrt{a^2-x^2},\quad |x|<a,\\ u_2(x,+0)-u_1(x,-0)&=-\sum_{k=1}^{N}B_{N+k}\frac{U_{2k-1}(x/a)}{2k}\sqrt{a^2-x^2},\quad |x|<a.\end{aligned} \tag{48a,b}$$

It should be noted that the eigenvectors B_j obtained from the homogeneous system (47) are determinate within an arbitrary multiplicative constant. Consequently (48) gives only the relative shape rather than the actual value of the crack opening.

Table 1
On the convergence of the calculated instability load $(\epsilon_0)_{cr}$ and phase angle $\psi(a)$, $v = 0.3$ (Fig. 1)

N	$h/a = 0.05$, $\gamma h = 0$		$h/a = 0.3$, $\gamma h = -2.3026$	
	$(\epsilon_0)_{cr}$	$\psi(a)$ (degree)	$(\epsilon_0)_{cr}$	$\psi(a)$ (degree)
2	0.001916	−25.52	0.04027	−37.82
4	0.001906	−37.30	0.03672	−42.15
8	0.001921	−39.12	0.03671	−42.36
16	0.001921	−39.07	0.03671	−42.37
32	0.001921	−39.07	0.03671	−42.39

Similarly by using (42) and by observing that (26a) and (26b) represent $\sigma^*_{yy}(x,0)$ and $\sigma^*_{xy}(x,0)$ outside $(|x| > a)$ as well as within $(|x| < a)$ the crack, the stress intensity factors may be evaluated as

$$K_I(a) = \lim_{x\to a}\sqrt{2\pi(x-a)}\sigma^*_{yy}(x,0) = -\mu_1 D_1\sqrt{\pi a}\sum_{j=1}^{N} B_j = K_I(-a),$$
$$K_{II}(a) = \lim_{x\to a}\sqrt{2\pi(x-a)}\sigma^*_{xy}(x,0) = -\mu_1 D_2\sqrt{\pi a}\sum_{j=1}^{N} B_{N+j} = -K_{II}(-a). \quad (49a,b)$$

Again, because of the arbitrariness in the magnitude of the eigenvector B_k at $\epsilon_0 = (\epsilon_0)_{cr}$ only the relative values of the stress intensity factors can be evaluated. This means that the phase angle $\psi(a)$ which defines the mode mixity may be evaluated exactly:

$$\psi(a) = \tan^{-1}\frac{K_{II}(a)}{K_I(a)} = \tan^{-1}\left(D_2\sum_{j=1}^{N} B_{N+j}/D_1\sum_{j=1}^{N} B_j\right). \quad (50)$$

Once N is prescribed, using iteration (47) can be solved for ϵ_0 within any desired degree of accuracy. Table 1 shows some results that give an idea about the convergence of the calculated quantities, in this case the instability load $(\epsilon_0)_{cr}$ and the phase angle $\psi(a)$. The results are obtained for a homogeneous half plane $(\gamma h = 0)$ [3] with a crack parallel to the boundary and for a graded coating ($\gamma h = -2.3026$ or $\mu_2(h)/\mu_1 = 0.1$) with an interface crack. The convergence seems to be very good. For as small as $N = 8$ (a total of 16 unknown coefficients), the results appear to be quite accurate.

4. The postbuckling analysis

From the physics of the problem it is clear that as long as the applied load ϵ_0 is below the critical value $(\epsilon_0)_{cr}$, the crack will remain closed and the stress intensity factors and the strain energy release rate will be zero. The problems of interest in this study are, then, the determination of $(\epsilon_0)_{cr}$ and the postbuckling analysis. The instability problem for a graded coating was considered in the previous section. To complete the fracture mechanics problem and to model such phenomena as subcritical crack growth and crack branching, the nonlinear postbuckling analysis also needs to be carried out. In this study this is done by using a finite element method based on the code FRAC2D (Kaya and Nied, 1993). The modified code uses special nonhomogeneous enriched 12-noded quadrilateral and 10-noded triangular cubic elements for the crack tip region which makes it possible to calculate the stress intensity factors directly. The "enriched"

[3] See (Chiu, 2000), Appendix H for the solution of the half plane problem where the kernels k_{ij} of the integral equations (26) are obtained in closed form, simplifying the problem quite considerably.

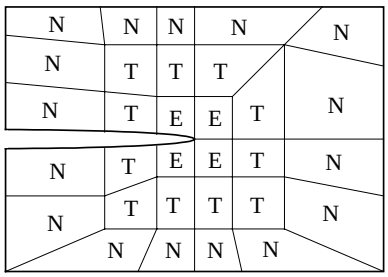

Fig. 3. Schematic description of the element assignment around the crack tip: E, enriched element; T, transition element and N, regular nonlinear element.

finite element method includes the effect of crack tip singularity in the conventional finite element displacement formulation. For the rest of the composite medium geometrically nonlinear nonhomogeneous 12-noded quadrilateral and 10-noded triangular cubic isoparametric elements are used. The nonhomogeneity is accounted for by prescribing the thermomechanical material constants at the Gaussian integration points. One important issue in integrating enriched and nonlinear finite elements is the inter-element compatibility between these two types of elements which can be handled by introducing a layer of transition elements and a zeroing function (Fig. 3). Thus, the general form of the components of the displacement vector within the jth element may be expressed as

$$u_{1j} = \sum_{k=1}^{M} N_k u_{1j}^k + Z\left[K_{\mathrm{I}}\left(f_{1j} - \sum_{k=1}^{M} N_k f_{1j}^k\right) + K_{\mathrm{II}}\left(g_{1j} - \sum_{k=1}^{M} N_k g_{1j}^k\right)\right], \tag{51a}$$

$$u_{2j} = \sum_{k=1}^{M} N_k u_{2j}^k + Z\left[K_{\mathrm{I}}\left(f_{2j} - \sum_{k=1}^{M} N_k f_{2j}^k\right) + K_{\mathrm{II}}\left(g_{2j} - \sum_{k=1}^{M} N_k g_{2j}^k\right)\right], \tag{51b}$$

where u_{1j}^k and u_{2j}^k are the nodal point displacements, N_k is the appropriate interpolation function, M is the number of nodes, K_{I} and K_{II} are the modes I and II stress intensity factors, f_{ij} and g_{ij} correspond to the asymptotic expressions for the displacements near the crack tip and Z is the zeroing function. [4] The function Z is defined in such a way that $Z = 1$ in the enriched elements, is a linear function in the transition elements and $Z = 0$ for the remaining nonlinear elements (Fig. 3). Similarly, to overcome the incompatibility in the strain-displacement relations and to attain better computational convergence it is also assumed that

$$\epsilon_{rs} = \tfrac{1}{2}[u_{r,s} + u_{s,r} + (1 - Z)u_{k,r}u_{k,s}], \quad (k, r, s) = (1, 2). \tag{52}$$

In (51) the unknowns are $2M$ nodal point displacements and two stress intensity factors K_{I} and K_{II}. For example, for a 12-noded quadrilateral element there are 26 unknowns.

The postbuckling problem under consideration is nonlinear and is solved by using an incremental-iterative procedure. That is, instead of applying the full amount of the external load in one step, a series of smaller load increments are applied. For each load increment an approximate solution is obtained by referring all variables to a previously known equilibrium configuration and by linearizing the resulting equations. The solution is then improved by iteration (see Chiu, 2000 for details).

[4] In (51) the subscripts 1 and 2 refer to the x and y components of the corresponding quantities.

5. Results and discussion

5.1. The instability problem

Some sample results for the instability problem described in Fig. 1 and obtained by following the procedure outlined in Section 3 are given in Figs. 4–12. In all the examples discussed in this section the Poisson's ratio is assumed to be 0.3. The hypothetical nonhomogeneity parameters γh used in the examples correspond to the material stiffness parameter as follows (Fig. 1):

$$\gamma h = 3.0 \rightarrow \mu_2(h)/\mu_1 = 20.09,$$
$$\gamma h = 2.3026 \rightarrow \mu_2(h)/\mu_1 = 10,$$
$$\gamma h = -2.3026 \rightarrow \mu_2(h)/\mu_1 = 0.1,$$
$$\gamma h = -3.0 \rightarrow \mu_2(h)/\mu_1 = 0.04979,$$

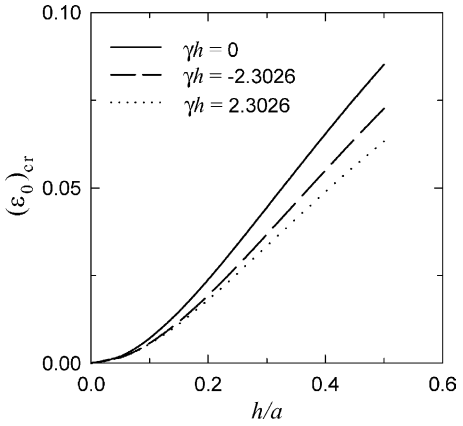

Fig. 4. Instability strain $(\epsilon_0)_{cr}$ as a function of h/a.

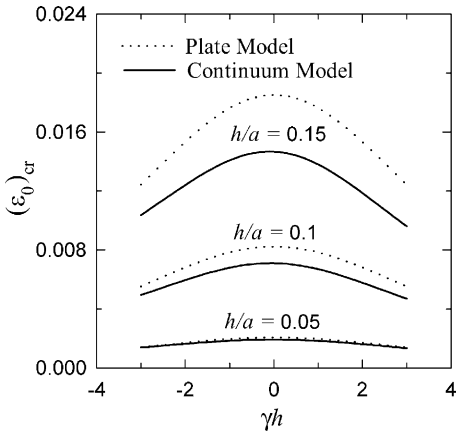

Fig. 5. Instability strain $(\epsilon_0)_{cr}$ as a function of coating nonhomogeneity γh.

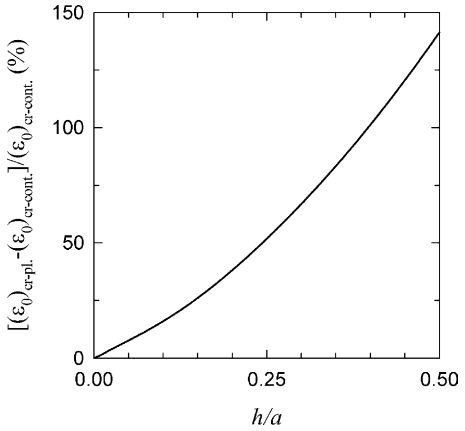

Fig. 6. The difference between the instability strain predicted by plate approximation $(\epsilon_0)_{\text{cr-pl.}}$ and that by continuum model $(\epsilon_0)_{\text{cr-cont.}}$ as a function of h/a.

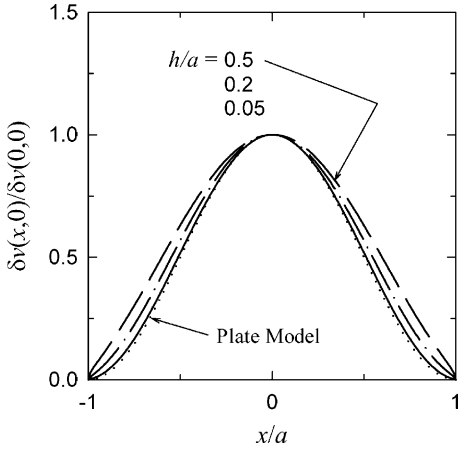

Fig. 7. Normalized crack opening displacements for $\gamma h = -2.3026$, $\delta v(x,0) = v_2(x,+0) - v_1(x,-0)$.

where $\mu_2(y) = \mu_1 \exp(\gamma y)$ (Fig. 1). Since $\gamma h = 0$ could not be substituted in the nonhomogeneous analysis due to numerical difficulties, also considered in calculations were the case of $\gamma h = 0.0001$ in the nonhomogeneous program and $\gamma h = 0$, the homogeneous half plane which was obtained independently (Chiu, 2000). This was done partly to verify the accuracy of the nonhomogeneous analysis and the related numerical procedure. The calculated values of the critical strain $(\epsilon_0)_{\text{cr}}$ and the phase angle $\psi(a)$ (at the crack tip $x = +a$) for $\gamma h = 0.0001$ and $\gamma h = 0$ are shown in Table 2. For a very wide range of the geometric stiffness constant h/a, the two sets of results are seen to be identical. [5]

[5] Table 2 indicates that the mode II stress intensity factor is negative. Since the material is homogeneous, $K_{\text{II}} < 0$ implies that the crack will grow toward the less stiff medium or the free surface.

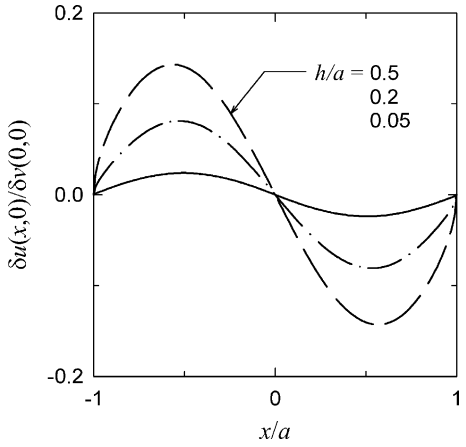

Fig. 8. Normalized crack opening displacements for $\gamma h = -2.3026$, $\delta u(x,0) = u_2(x,+0) - u_1(x,-0)$.

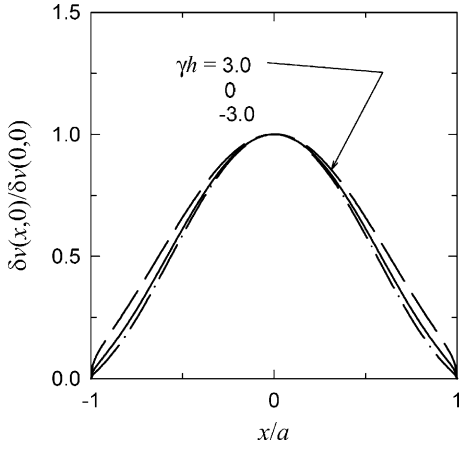

Fig. 9. Normalized crack opening displacements for $h/a = 0.3$, $\delta v(x,0) = v_2(x,+0) - v_1(x,-0)$.

The calculated critical strain $(\epsilon_0)_{cr}$ is shown in Fig. 4 as a function of geometric stiffness parameter h/a. It is seen that $(\epsilon_0)_{cr}$ is a monotonically increasing function of h/a and properly approaches zero as h/a goes to zero. [6] The figure also shows that regardless of the nature of coating nonhomogeneity, for all values of h/a the homogeneous medium requires a greater instability load to initiate buckling. Intuitively one would expect that the critical loads for $\gamma h > 0$ and $\gamma h < 0$ would bracket $(\epsilon_0)_{cr}$ for $\gamma h = 0$. The fact that this argument would be very misleading may be seen from Fig. 5 which shows the influence of material nonhomogeneity on the buckling strain $(\epsilon_0)_{cr}$ for $h/a = 0.05$, 0.1 and 0.15. Also shown in Fig. 5 is the critical strain obtained from the plate theory (see the Appendix A for closed form solution). The plate theory shows that $(\epsilon_0)_{cr}$ for the plate is an even function of γh and becomes maximum at $\gamma h = 0$. The critical strain given by the continuum theory shows the same trend as that given by the plate theory except that the maximum is

[6] In the case of plate approximation, near $h/a = 0$, $(\epsilon_0)_{cr} \sim (h/a)^2$ (see Hutchinson and Suo, 1992 and the Appendix A).

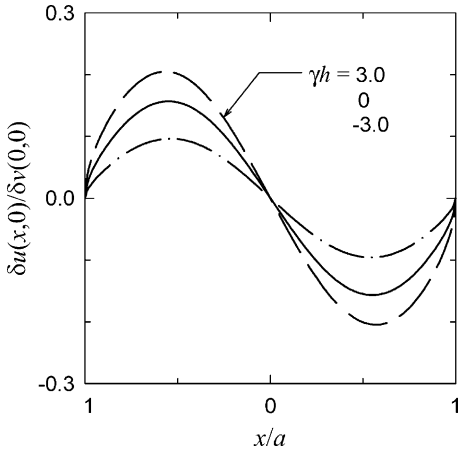

Fig. 10. Normalized crack opening displacements for $h/a = 0.3$, $\delta u(x,0) = u_2(x,+0) - u_1(x,-0)$.

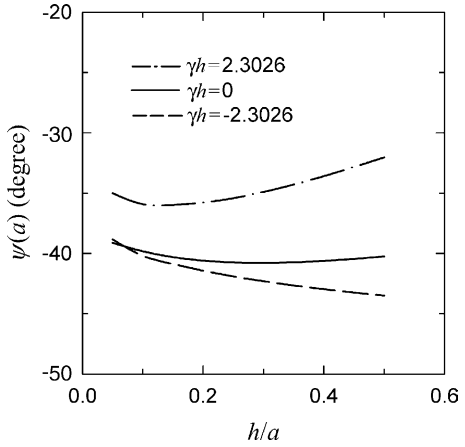

Fig. 11. Phase angle $\psi(a)$ for the interface crack at buckling instability as a function of h/a.

slightly shifted toward negative γh. [7] Note that for very small values of h/a, as expected, the results obtained from plate and continuum theories are indistinguishable, whereas for greater values of h/a the difference could be very significant. Also, for all values of h/a and γh the plate theory predicts consistently higher values for critical strain. For $\gamma h = 0$ this may also be seen from Fig. 6 which shows the difference between the critical strains calculated from the continuum and the plate models. The difference may be attributed to the fact that at $x = \mp a$ the plate is assumed to have built-in ends (that is, ends with artificially imposed high constraints) whereas the continuum theory imposes no such predetermined constraints.

Figs. 7–10 shows the crack opening displacements for some fixed values of γh and h/a normalized with respect to the corresponding values of $v_2(0,+0) - v_1(0,-0) = \delta v(0,0)$. From the figures it may be seen that the shear components of the relative crack openings $\delta u(x,0)$ are considerably smaller and more sensitive to

[7] As h/a goes to zero $(\epsilon_0)_{cr}$ given by the continuum theory, too, becomes an even function of γh in the sense that for $h/a \to 0$ the continuum results converge to plate results.

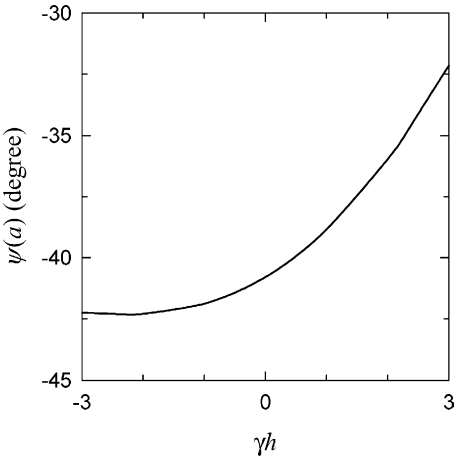

Fig. 12. The influence of coating nonhomogeneity γh on the phase angle $\psi(a)$ for the interface crack at buckling instability, $h/a = 0.3$.

Table 2
Critical strain and phase angle for a homogeneous half-space containing a crack parallel to the surface subjected to fixed-grip compression as described in Fig. 2 with $\gamma h = 0$ and $\gamma h = 0.0001$

h/a	Critical strain $(\epsilon_0)_{cr}$		Phase angle ψ (degree)	
	$\gamma h = 0.0001$	$\gamma h = 0$	$\gamma h = 0.0001$	$\gamma h = 0$
0.05	0.001921	0.001921	−39.1	−39.1
0.1	0.007103	0.007103	−39.8	−39.8
0.15	0.01467	0.01467	−40.3	−40.3
0.2	0.02381	0.02381	−40.6	−40.6
0.25	0.03388	0.03388	−40.7	−40.7
0.3	0.04439	0.04439	−40.8	−40.8
0.35	0.05498	0.05498	−40.7	−40.7
0.4	0.06540	0.06540	−40.6	−40.6
0.45	0.07551	0.07551	−40.5	−40.5
0.5	0.08520	0.08520	−40.3	−40.3

h/a and γh than the corresponding normal crack openings $\delta v(x, 0)$. Fig. 7 also shows the normal crack opening obtained from the plate model. Again, as h/a decreases the continuum results are seen to approach the plate results. Figs. 9 and 10 show the crack openings for a constant h/a and for various coating stiffnesses. The trends are qualitatively similar to that shown in Figs. 7 and 8 in that as the coating stiffness (h/a or γh) decreases the crack openings also tend to decrease. Some examples showing the dependence of the phase angle on h/a and γh are given in Figs. 11 and 12.

Some sample results for the weakened interface model are shown in Figs. 13 and 14. Fig. 13 describes the dependence of $(\epsilon_0)_{cr}$ on γh for various values of geometric stiffness h/a and (dimensionless) bridging constant as/μ_1 where it is assumed that $s_1 = s_2 = s$ (see Section 3.2). Also given in the figure are the results for fully developed cracks, i.e., for $s = 0$. It may be observed that as s decreases, the results approach that given by the crack problem ($s = 0$), the stiffer coating (or greater h/a) requires higher instability load $(\epsilon_0)_{cr}$ and generally the critical strain $(\epsilon_0)_{cr}$ is much more sensitive to the coating nonhomogeneity for negative values of γh. Fig. 14 shows the dependence of $(\epsilon_0)_{cr}$ on the bridging constant as/μ_1 for two practical material pairs, namely a metal substrate (Ti–6Al–4V, $E = 116.7$ GPa, $\nu = 0.3$) and a metal/zirconia ($E = 151$ GPa, $\nu = 0.3$) graded coating ($\gamma h = 0.2577$) and a metal substrate (Rene-41 alloy, $E = 219.7$ GPa, $\nu = 0.3$) and a metal/zirconia graded coating ($\gamma h = -0.3750$). From the figure it may be seen that $(\epsilon_0)_{cr}$ remains

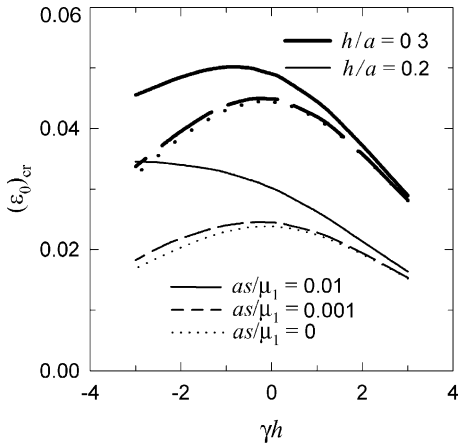

Fig. 13. Instability strain $(\epsilon_0)_{cr}$ as a function of coating nonhomogeneity γh for the graded coating/homogeneous substrate containing a weakened interface under fixed-grip compression.

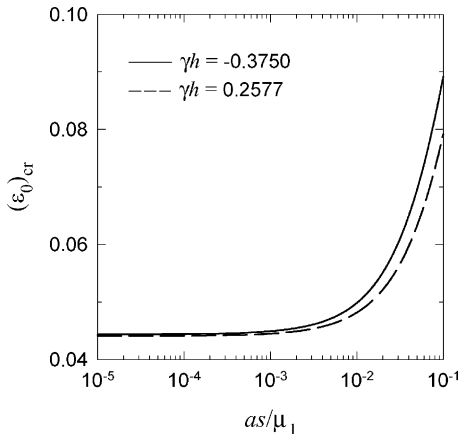

Fig. 14. The influence of the normalized bridging constant as/μ_1 on the instability strain $(\epsilon_0)_{cr}$ for the weakened interface, $h/a = 0.3$.

nearly constant for $as/\mu_1 < 10^{-3}$ and increases quite rapidly with increasing bridging coefficient for $as/\mu_1 > 10^{-2}$.

It should be observed that the results obtained in this study for the weak interface model and shown in Figs. 13 and 14 are found by solving the corresponding continuum eigenvalue problem. For a fixed value of the bridging coefficient as/μ_1, as expected, the "effective length" a is influenced by the spring constant s in such a way that increasing s corresponds to decreasing effective length.

5.2. Postbuckling analysis

The nonlinear numerical procedure used in the postbuckling analysis of graded coatings was described in Section 4. The benchmark results for $(\epsilon_0)_{cr}$ were obtained analytically and were discussed in the previous section (Section 5.1). In this section the critical strain $(\epsilon_0)_{cr}$ is also obtained as the bifurcation point in the postbuckling analysis. The results obtained from the constant strain loading described in Fig. 1 are shown

in Figs. 15–18. In the numerical analysis, of necessity, the length l and the thickness h_s of the substrate had to be finite. Thus, the relative dimensions used in the calculations were assumed to be

$$\frac{h_s}{h_c} = 30, \quad \frac{2a}{h_c} = 40, \quad \frac{2l}{h_c} = 200,$$

where h_c is the coating thickness. The test results obtained by varying h_s/h_c and $2l/h_c$ showed that the dimensions used were sufficiently large to simulate the semi-infinite medium accurately. Note that similar to elastica problems in this problem, too, the load-displacement path cannot be determined in a straightforward manner by using the incremental-iterative procedure starting from zero external load (see Chiu, 2000 for the numerical solution of the elastica problem and its comparison with the exact solution). To start the procedure first a small transverse load is applied to the coating at the point $x = 0$, $y = +0$ to induce an initial crack opening. The load is then removed at a later stage of the incremental loading history to obtain an equilibrium point in the postbuckling regime for the original problem. Starting from this equilibrium point the load path is then constructed by using the incremental-iterative technique. For various values of

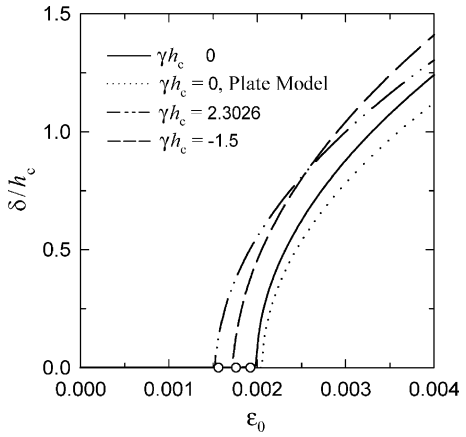

Fig. 15. Crack opening displacement δ/h_c at the center of crack as a function of compressive strain ϵ_0, the circles on the ϵ_0 axis are the instability strains $(\epsilon_0)_{cr}$ calculated from the analytical stability solution.

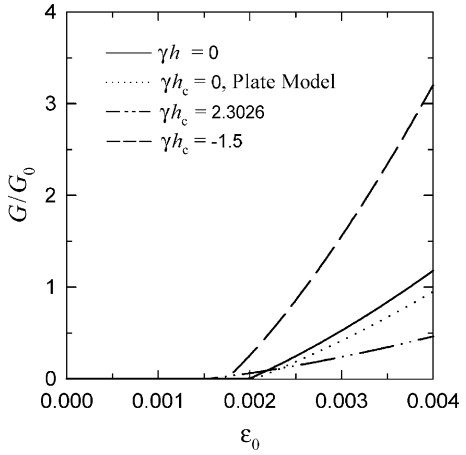

Fig. 16. Strain energy release rate G/G_0 as a function of compressive strain ϵ_0, $G_0 = (1 - \nu_s^2)K_0^2/E_s$, $K_0 = E_s\epsilon_1\sqrt{\pi h_c}$, $\epsilon_1 = 0.002$.

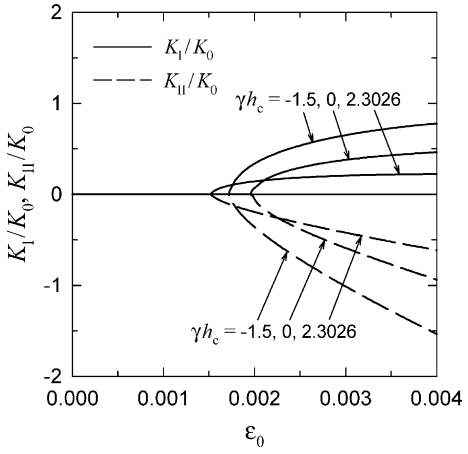

Fig. 17. Modes I and II stress intensity factors K_I and K_{II} as functions of compressive strain ϵ_0, $K_0 = E_s\epsilon_1\sqrt{\pi h_c}$, $\epsilon_1 = 0.002$.

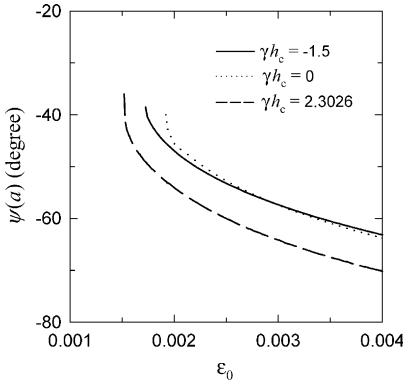

Fig. 18. Phase angle as a function of compressive strain ϵ_0.

the coating nonhomogeneity parameter γh_c the crack opening displacement at $x = 0$ (defined by δ) is shown in Fig. 15. Note that as ϵ_0 is increased δ remains zero until a critical loading $(\epsilon_0)_{cr}$ is reached, then the load path bifurcates. For each value of γh_c $(\epsilon_0)_{cr}$ obtained from the analytical solution is also shown in the figure (the small circle). The agreement between the two sets of calculated results appears to be very good. For $\gamma h_c = 0$ the figure also shows the crack opening δ obtained from the plate model. The difference between the plate and the continuum results seems to be rather insignificant. This is due to the relatively small geometric stiffness parameter $(h_c/a = 0.05)$ used in the example. Again, it may be observed that in the postbuckling regime, too, for a given crack opening the plate model requires a greater compressive strain ϵ_0 than the continuum theory. This is also partly due to the greater end constraints assumed in the plate theory and is consistent with the results given in Fig. 5.

For the example considered, the dependence of the strain energy release rate G and the stress intensity factors K_I and K_{II} on the external load ϵ_0 is shown in Figs. 16 and 17. It may be seen that for $\epsilon_0 < (\epsilon_0)_{cr}$ G, K_I and K_{II} are zero and for $\epsilon_0 > (\epsilon_0)_{cr}$ material nonhomogeneity constant γh_c and ϵ_0 have a significant influence on the fracture mechanics parameters G, K_I and K_{II}. By and large the relative trends seem to conform to intuitively expected results, namely G corresponding to $\gamma h_c = 0$ is bracketed by the strain energy release rates obtained from $\gamma h_c < 0$ and $\gamma h_c > 0$ and G increases with decreasing coating stiffness γh_c.

By examining the results for $\gamma h_c = 0$ given in Figs. 15 and 16, it may be seen that δ and G predicted by the plate model for a given ϵ_0 are consistently smaller than that obtained from the continuum theory. This, again, is due to the artificially imposed end constraints in the plate model. From a design viewpoint the plate model seems to be nonconservative and requires caution in applications. Fig. 17 shows that K_{II} is the dominant stress intensity component. This may also be seen from Fig. 18 which shows the phase angle $\psi(a)$ in the postbuckling regime. Relatively high and negative K_{II} implies a strong possibility of crack kinking towards the free surface. Perhaps a more practical approach to nonplanar crack growth would be either comparing the calculated G with the mode-mixity-dependent fracture toughness G_c or by using a maximum stress-based rupture theory at the crack tip region.

6. Concluding remarks

The problems of instability and postbuckling behavior of a graded coating bonded to a homogeneous substrate with an interface crack or a highly damaged interfacial zone and subjected to uniform in-plane compressive strain ϵ_0 are studied by using a kinematically nonlinear continuum theory and the von Karman plate model. The shear modulus of the coating is assumed to be $\mu_c = \mu_s \exp(\gamma y)$, where μ_s is the modulus of the substrate and γh_c is the material nonhomogeneity constant which may be positive or negative. Following are some conclusions:

1. Regardless of the sign and magnitude of γh_c the critical compressive strain at bifurcation $(\epsilon_0)_{cr}$ is (approximately) highest for $\gamma h_c = 0$.
2. Because of the artificially imposed end constraints, the plate model requires $(\epsilon_0)_{cr}$ that is consistently greater than that required by the continuum theory for all values of γh_c and the difference in $(\epsilon_0)_{cr}$ given by the two theories increases with increasing h_c/a.
3. For buckling the interface defect need not be a fully developed crack. Sufficiently small values of the bridging constant as/μ_1 and the geometric stiffness parameter h_c/a ($2a$ being the size of the flawed zone) could also lead to buckling.
4. Good agreement is found between the bifurcation points or $(\epsilon_0)_{cr}$ obtained from the analytical solution of the related eigenvalue problem and from the numerical solution of the postbuckling problem.
5. In the postbuckling regime for a given crack opening the plate model requires greater compressive strain $(\epsilon_0)_{cr}$ than the continuum theory.
6. For a given value of loading in the postbuckling regime ($\epsilon_0 > (\epsilon_0)_{cr}$) the strain energy release rate and the crack opening predicted by the plate model are consistently smaller than that obtained from the continuum theory, implying that generally the results given by the plate model are nonconservative.
7. In the postbuckling regime the mode II stress intensity factor is dominant and negative, implying that the crack may tend to kink toward the free surface.

Appendix A. The plate model

The plate model described in this appendix and used to obtain the approximate results in this study are essentially the same as that given by Hutchinson and Suo (1992).

A.1. The stability analysis

In the stability analysis the delaminated part of the graded coating ($-a < x < a$, $0 < y < h$, Figs. 1 and 19) is approximated by a "plate" with built-in ends and is subjected to a uniform compressive strain ϵ_0. The elastic constants of the plate are given by

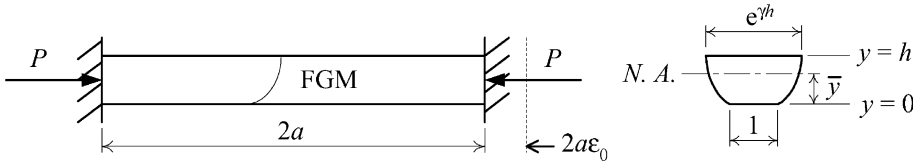

Fig. 19. Configuration of the column with transformed cross-section.

$$v_1 = v_2 = v = \text{constant}, \quad E_2^*(y) = E_1^* e^{\gamma y}, \quad E_1^* = \frac{E_1}{1-v^2}, \qquad 0 < y < h, \tag{A.1}$$

where $E_1 = 2\mu_1(1+v)$ is the Young's modulus of the substrate (Fig. 1). The analysis is carried out by using the standard "Euler-column" approach with transformed cross-section technique accounting for the material nonhomogeneity. From (A.1) and Fig. 19 the position of the neutral axis and the transformed area moment of inertia may be determined as

$$\bar{y} = \frac{\int y\,dA}{A} = \frac{\int_0^h y e^{\gamma y}\,dy}{\int_0^h e^{\gamma y}\,dy} = \frac{\gamma h e^{\gamma h} - e^{\gamma h} + 1}{\gamma(e^{\gamma h} - 1)}, \tag{A.2}$$

$$I_t = \int_0^h (y-\bar{y})^2\,dA = \int_0^h (y-\bar{y})^2 e^{\gamma y}\,dy = \frac{(e^{\gamma h}-1)^2 - (\gamma h)^2 e^{\gamma h}}{\gamma^3(e^{\gamma h}-1)}. \tag{A.3}$$

The axial-force P corresponding to ϵ_0 and the critical buckling load (per unit width) may then be expressed as

$$P = \int E^*(y)\epsilon_0\,dA = \int_0^h E_1^* e^{\gamma y}\epsilon_0\,dy = E_1^*\epsilon_0(e^{\gamma h}-1)/\gamma, \tag{A.4}$$

$$P_{cr} = \frac{4\pi^2 E_1^* I_t}{(2a)^2}. \tag{A.5}$$

From (A.3)–(A.5) it then follows that

$$(\epsilon_0)_{cr} = \pi^2\left(\frac{h}{a}\right)^2\left[\frac{1}{(\gamma h)^2} - \frac{1}{(e^{\gamma h} + e^{-\gamma h} - 2)}\right], \quad \gamma \neq 0. \tag{A.6}$$

It is seen that for the particular nonhomogeneity considered $(\epsilon_0)_{cr}$ is an even function of the parameter γh. For the homogeneous plate, that is, for $\gamma = 0$, it can be shown that

$$(\epsilon_0)_{cr} = \frac{\pi^2}{12}\left(\frac{h}{a}\right)^2. \tag{A.7}$$

A.2. The postbuckling analysis

By following Hutchinson and Suo (1992) the crack problem associated with the postbuckling of coating is formulated by coupling the von Karman plate with the split-beam approach (Fig. 20). It is assumed that the crack length $2a$ and the thickness of the substrate are very large in comparison with the coating thickness h. The membrane load N and bending moment M acting on the split-beam are obtained by using the nonlinear von Karman plate formulation. It is assumed that the thermomechanical properties of the

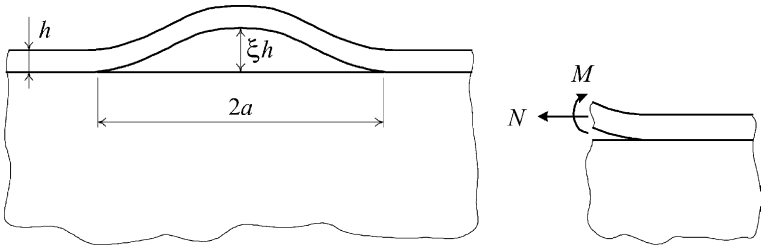

Fig. 20. Geometry of the one dimensional blister: (a) the buckled coating, (b) local loading of interface crack.

coating E, v and α are known functions of y. The location of the neutral axis and the bending stiffness are given by

$$\bar{y} = \frac{\int_0^h yE^*(y)\,\mathrm{d}y}{\int_0^h E^*(y)\,\mathrm{d}y}, \quad E^*(y) = \frac{E(y)}{1-v^2(y)}, \tag{A.8}$$

$$D = \int_0^h E^*(y)(y-\bar{y})^2\,\mathrm{d}y. \tag{A.9}$$

The buckling problem may then be formulated as

$$D\frac{\mathrm{d}^4 v}{\mathrm{d}x^4} + \Delta N\frac{\mathrm{d}^2 v}{\mathrm{d}x^2} = 0, \quad \Delta N = P - N, \tag{A.10}$$

$$v|_{x=\mp a} = 0, \quad \left.\frac{\mathrm{d}v}{\mathrm{d}x}\right|_{x=\mp a} = 0. \tag{A.11}$$

From (A.10) and (A.11) the deflection and the corresponding lowest eigenvalue (the buckling load) are found to be

$$v(x) = \frac{1}{2}\xi h\left(1+\cos\frac{\pi x}{a}\right), \quad \Delta N = P_{\mathrm{cr}} = \frac{\pi^2 D}{a^2}, \tag{A.12}$$

where $\xi = v(0)/h$ is the unknown amplitude and is determined by the condition that the membrane stress in the buckled coating is the same as the buckling stress giving

$$\int_{-a}^{a} \epsilon_{xx}\,\mathrm{d}x = 2a\left(\frac{P-P_{\mathrm{cr}}}{\lambda}\right), \quad \lambda = \int_0^h E^*(y)\,\mathrm{d}y. \tag{A.13}$$

The nonlinear strain ϵ_{xx} is given by

$$\epsilon_{xx} = \frac{1}{2}\left(\frac{\mathrm{d}v}{\mathrm{d}x}\right)^2. \tag{A.14}$$

From (A.12)–(A.14) it may be shown that

$$\xi = \frac{v(0)}{h} = \frac{4}{h}\left[\frac{D}{\lambda}\left(\frac{P}{P_{\mathrm{cr}}}-1\right)\right]^{1/2}. \tag{A.15}$$

The bending moment M at $x = a$ and the resultant force N are obtained as

$$M = D\frac{\mathrm{d}^2 v}{\mathrm{d}x^2}\bigg|_{x=a} = \frac{\pi^2 Dh}{2a^2}\xi, \quad N = P - P_{\mathrm{cr}}. \tag{A.16}$$

By using (A.16) from the split-beam solution the strain energy release rate is then found to be

$$G = \frac{P^2}{2\lambda}\left(1 - \frac{P_{\mathrm{cr}}}{P}\right)\left(1 + 3\frac{P_{\mathrm{cr}}}{P}\right). \tag{A.17}$$

The in-plane compressive load P that appears in (A.15) and (A.17) is dependent on ϵ_0 and may be determined as

$$P = -\int_0^h \sigma_{xx}\,\mathrm{d}y = \int_0^h \frac{E(y)}{1 - \nu^2(y)}\epsilon_0\,\mathrm{d}y. \tag{A.18}$$

References

Bao, G., Cai, H., 1997. Delamination cracking in functionally graded coating/metal substrate systems. Acta Materialia 45, 1055–1066.

Bottega, W.J., Maewal, A., 1983. Delamination buckling and growth in laminates. Journal of Applied Mechanics 50, 184–189.

Chai, H., Knauss, W.G., Babcock, C.D., 1983. Observation of damage growth in compressively loaded laminates. Experimental Mechanics 23, 329–337.

Chen, Y.F., Erdogan, F., 1996. Interface crack problem for a nonhomogeneous coating bonded to a homogeneous substrate. Journal of the Mechanics and Physics of Solids 44, 771–787.

Chiu, T.-C., 2000. Buckling of graded coatings—a continuum model. Ph.D. Dissertation, Lehigh University, Bethlehem, Pennsylvania.

Delale, F., Erdogan, F., 1988. Interface crack in a nonhomogeneous elastic medium. International Journal of Engineering Science 26, 559–568.

Erdogan, F., Joseph, P.F., 1989. Toughening of ceramics through crack bridging by ductile particles. Journal of the American Ceramic Society 72, 262–270.

Evans, A.G., Hutchinson, J.W., 1984. On the mechanics of delamination and spalling in compressed films. International Journal of Solids and Structures 20, 455–466.

Evans, A.G., Crumley, G.B., Demaray, R.E., 1983. On the mechanical behavior of brittle coatings and layers. Oxidation of Metals 20, 193–216.

Evans, A.G., He, M.Y., Hutchinson, J.W., 1997. Effect of interface undulations on the thermal fatigue of thin films and scales on metal substrates. Acta Materialia 45, 3543–3554.

Garg, A.C., 1988. Delamination—a damage mode in composite structures. Engineering Fracture Mechanics 29, 557–584.

Holt, J.B., Koizumi, M., Hirai, T., Munir, Z.A. (Eds.), 1993. Ceramic Transactions—Functionally Gradient Materials, Vol. 34, American Ceramic Society, Westerville, Ohio.

Hutchinson, J.W., Suo, Z., 1992. Mixed mode cracking in layered materials. In: Hutchinson, J.W., Wu, T.Y. (Eds.), Advances in Applied Mechanics, Vol. 29, Academic Press, New York, pp. 63–191.

Ilschner, B., Cherradi, N. (Eds.), 1995. Proceedings of the 3rd International Symposium on Structural and Functionally Gradient Materials, Presses Polytechniques et Universitaires, Romandes, Lausanne, Switzerland.

Kaya, A.C., Nied, H.F., 1993. Interface fracture analysis of bonded ceramic layers using enriched finite elements. Ceramic Coatings. In: Kokini, K. (Ed.), The 1993 ASME Winter Annual Meeting, New Orleans, Louisiana, MD, Vol. 44, pp. 47–71.

Kaysser, W.A., (Ed.), 1999. Materials Science Forum—Functionally Graded Materials, Vol. 308–311, Trans Tech Publications.

Keer, L.M., Nemat-Nasser, S., Oranratnachai, A., 1982. Surface instability and splitting in compressed brittle elastic solids containing crack arrays. Journal of Applied Mechanics 49, 761–767.

Madenci, E., Westmann, R.A., 1991. Local delamination buckling in layered systems. Journal of Applied Mechanics 58, 157–165.

Malvern, L.E., 1969. Introduction to the Mechanics of a Continuous Medium. Prentice-Hall, Eaglewood Cliffs, NJ.

Miyamoto, Y., Kaysser, W.A., Rabin, B.H., Kawasaki, A., Ford, R.G. (Eds.), 1999. Functionally Graded Materials. Kluwer Academic Publishers, The Netherlands.

Niino, M., Hirai, T., Watanabe, R., 1987. The functionally gradient materials. Japan Society of Composite Materials 13, 257.

Nilsson, K.-F., Giannakopoulos, A.E., 1990. Finite element simulation of delamination growth. In: Aliabadi, M.H., Brebbia, C.A., Cartwright, D.J. (Eds.), 1st International Conference on Computer Aided Assessment and Control of Localized Damage, Vol. 2, Springer-Verlag, Portsmouth, UK, pp. 299–313.

Nilsson, K.-F., Thesken, J.C., Sindelar, P., Giannakopoulos, A.E., Storåkers, B., 1993. A theoretical and experimental investigation of buckling induced delamination growth. Journal of the Mechanics and Physics of Solids 41, 749–782.

Nusier, S.Q., Newaz, G., 1998. Crack initiation in thermal barrier coatings due to interface asperity. In: Newaz, G.M., Gibson, R.F. (Eds.), Proceedings of the 8th Japan-US Conference on Composite Materials, pp. 417–426.

Peck, S.O., Springer, G.S., 1991. The behavior of delaminations in composite plates-analytical and experimental results. Journal of Composite Materials 25, 907–929.

Shiota, I., Miyamoto, Y. (Eds.), 1997. FGM '96, Proceedings of the 4th International Symposium on Functionally Graded Materials, Elsevier, Amsterdam.

Trumble, K., Bowman, K., Reimanis, I., Sampath, S. (Eds.), 2001. Functionally Graded Materials 2000, Ceramic Transactions, Vol. 114, American Ceramics Society, Westerville, Ohio.

Wang, W.-X., Takao, Y., 1995. Load buckling of a layer bonded to a half-space with an interface crack. Journal of Applied Mechanics 62, 64–70.

Wang, W.-X., Shen, W., Takao, Y., Shen, Z., Chen, P.-H., 1991. An analysis of compressive stability of elastic solids containing a crack parallel to the surface. Engineering Fracture Mechanics 40, 1023–1033.

Whitcomb, J.D., 1989. Three-dimensional analysis of a postbuckled embedded delamination. Journal of Composite Materials 23, 862–889.

Yamanouchi, M., Koizumi, M., Hirai, T., Shiota, I. (Eds.), 1990. FGM '90, Proceedings of the 1st International Symposium on Functionally Gradient Materials, FGM Forum, Tokyo, Japan.